International Research Journal of Innovations in Engineering and Technology (IRJIET)

ISSN (online): 2581-3048
Volume 9, Issue 11, pp 99-116, November-2025
https://doi.org/10.47001/IRJIET/2025.911013

Effect of Coastal Dynamics on Interstitial Hydraulics in Beach Sediments

Okuroghoboye Diepreye Itugha

Department of Civil Engineering, Federal University Otuoke, 400 University Boulevard, Otuoke, PMB 126, Bayelsa State, Nigeria. E-mail: diepitu@yahoo.com

***Abstract* - Results from the field experiments to investigate plume movement and solute transport caused by strong semidiurnal-tides in beach sand are presented. Field observations of the evolved solute plumes reveal a uniquely conical shape. The vertical and horizontal cross-sections of the contaminated areas were measured in the field. The digital images were processed for spatial dimensions and the colour intensity records were converted to concentration using calibration techniques. Solute transport described by the plumes along the vertical cross-sections of the vadose-zone was found to be non-Gaussian, differing from that in the horizontal cross-sections. Fully developed two-dimensional (2D) plumes are used to account for the contaminant movement and transport in the sediments. We describe the influence of effective radial dispersion coefficient using moment's analysis, which can be applied to the advective-dispersion-equation (ADE) in cylindrical coordinates. A Gaussian model was also applied to individual plumes to determine the longitudinal (vertical), transverse (horizontal) flow cross-sections and concentration dataset. The effective radial hydrodynamic dispersion coefficients varied from $6.141x10^{-06}m^2/hr$ to $4.16148x10^{-05}m^2/hr$ within the mean radial distance of about 0.25m and $3.475x10^{-3}m/hr$ in pore-fluid flow. The quantitative results from the calibration and analytic processes will be useful benchmark for prediction, validation and sensitivity studies, such as involving solute dispersion arising from spatial fluctuations of the velocity field due to tidal changes affecting the morphology of the River Mersey Estuary (RME).**

Keywords: Coastal dynamics, visual scaling technique (VST), dispersivity, River Mersey Estuary (RME), hydraulics, concentration.

I. Introduction

Solute transport at water/sediment interface is an important process that determines the interactions between surface water, sediments, and groundwater. Previous tracer studies reveal that the solute transport occurs within the range from 0.01m/hr to $2.958x10^{-3}m/hr$ in coastal and marine underwater environment (Sudicky *et al* 1983). The solute transport in the inter-tidal areas is particularly relevant to contaminated sediments. For example, high concentrations of PAH and PCB have been observed in fine sediments of the inter-tidal areas near the river bank of the Mersey Estuary (Rogers, 2002; King *et al*, 2004). Understanding of the mechanism as well as reliable prediction of the solute transport in inter-tidal areas can improve the remediation work and future marine energy installations (e.g. tidal barrages, etc.). On the other hand, the Mersey Estuary has a high tide range (±5m). The beach areas undergo regular alternations between unsaturated and saturated zones in each tidal cycle. The beaches can serve as ideal sites to investigate the solute transport in the inter-tidal area.

The use of the conservative dyes to study the behavior associated to the movement of the dissolved substances in interstitial surroundings is prevalent (Lanyon *et al.* 1982; Fetter, 1999; Diaw *et al*, 2001). Most of the previous studies, however, dealt with the contaminant transport in groundwater aquifers. These differ from the present study which investigates the movement of the pollutant plumes in beach-sand vadose zone. A review on the groundwater behavior in sandy beaches with the relationship between tides and beach water-tables can be found in Baird and Horn (1996), Li and Jiao (2005) and Berkowitz *et al* (2008). Li *et al* (2000) and Boufadel *et al* (2006) showed that the oscillatory tides interacting with the groundwater flow fields do influence the dynamic regime of the hydrology in subsurface coastal foreshores. Dye tracers can therefore effectively account for the behaviour of migrant nutrients and/or contaminants to enable qualitative and quantitative evaluation of the mixing patterns generated by the tides in space and time. The conservative dye that is transmitted into the study field serves as optical tracer contaminant (Schincariol *et al* 1993; Swartz and Schwartz 1998; Rahman *et al* 2005; McNeil *et al* 2006).

A few modern dye trace imaging techniques have successfully been developed to investigate the plume formation, the movement and transport of solutes in the subsurface. The technique involves the use of, for example, probes, acoustic, positron emission tomography, Nuclear Magnetic Resonance (NMR), Photo-luminescent Volumetric Imaging, colored tracer imaging (Robbins, 1989; Sahimi,

International Research Journal of Innovations in Engineering and Technology (IRJIET)

ISSN (online): 2581-3048

Volume 9, Issue 11, pp 99-116, November-2025

https://doi.org/10.47001/IRJIET/2025.911013

1995; Khalili *et al*, 1998; Montemagno and Gray, 1995; Callaghan and Codd, 1998). However, to highlight the significance of monitoring natural flow patterns, the measuring techniques should not be invasive. According to Robbins (1989), solute monitoring devices are usually invasive, hence can distort the effective natural flow regime in subsurface environments. It may not be easily possible to obtain the quantitative concentration profiles in such environments (Precht and Huettel, 2004). Though several previous studies were able to collect the quantitative and qualitative data of the movement of solute plumes, these studies were mostly based on groundwater aquifer. The emphasis here is to use the fully developed plumes generated by strong tides to account for contaminant movement. To our best knowledge, measurements of full 2D plume shapes of this nature have not been reported and published previously.

In this study, the effects of tidally generated advective and diffusive transport of the contaminants at the water-sediment interface are investigated using in-situ measurements and calibration of the 2D plume images. The measurement and processing of the evolved 2-Dplume image from three sites are described in detail. Transport rate of solute at the water-sediment interfaceis analyzed using methods derived from moments and calibration. The hydrodynamic dispersion coefficients are estimated. The results are favorably compared to relevant previous studies.

II. Description of study area, experimental design, method and digital-image processing

2.1 Study site

All experimental sites are located at the coastal foreshores of the Liverpool Bay (outer estuary injection site and zone (OEIS-IZ)) and Narrows (narrows estuary injection site and zone (NEIS-IZ)) of the RME, NW England (53°26′N and 003°02′W) (see Fig. 1). The historic and socio-economic significance of the catchment, such as urban/industrial waste and sewage sludge discharge information, can be found in literatures (Jones, 2006; Rogers, 2002; King *et al*, 2004). The map in Fig. 1 illustrates the Outer and entrance to the Narrows of the estuary that is open to the Irish Sea at the Liverpool Bay. The water levels at the experimental sites are nearly the same as in the sea. During low tides, large portions of the intertidal foreshore are exposed. The median grain size (d_{50}) of the exposed foreshore varies spatially with the range from 0.196mm t o 0.259mm.Thestrongtides can reach about ±5m are while the mean tides vary at less than ±2m.

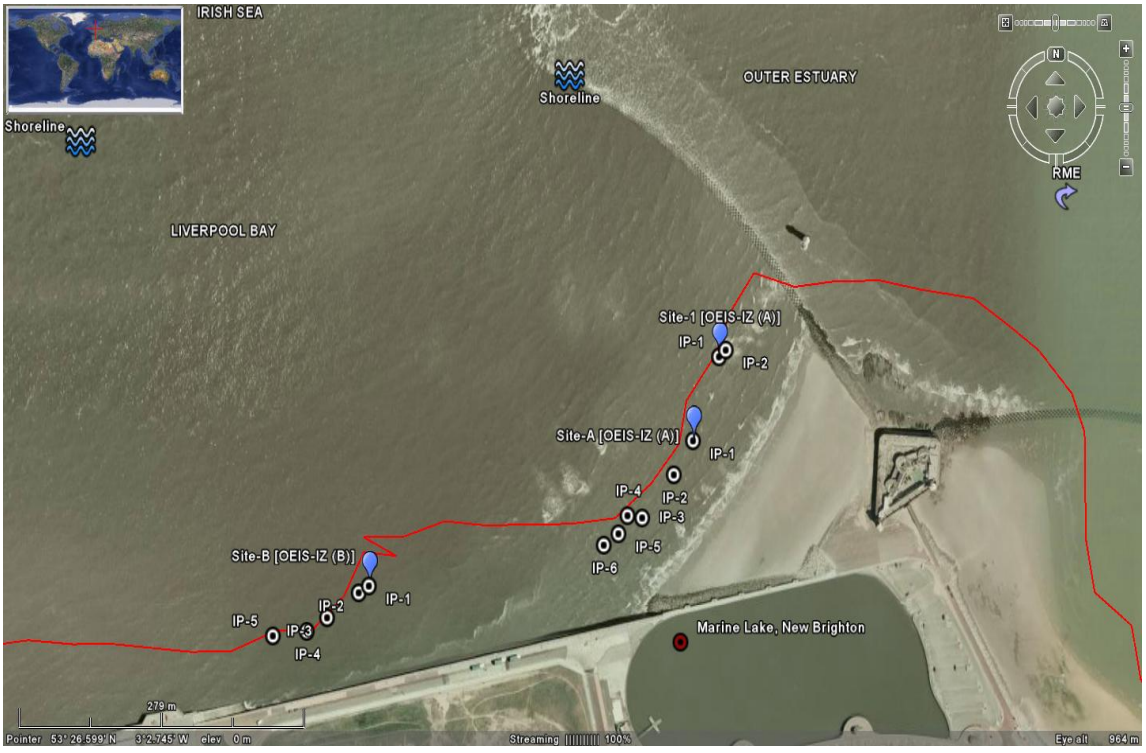

Figure 1: Area map showing some of the GPS injection zones and positions at outer RME with overview map

[Balloon – injection zone; Circle – injection point; Water-lines – shoreline at ebb-water; Line – area covered during experiments]

International Research Journal of Innovations in Engineering and Technology (IRJIET)

ISSN (online): 2581-3048

Volume 9, Issue 11, pp 99-116, November-2025

https://doi.org/10.47001/IRJIET/2025.911013

2.2 Experimental design, tracer applied and method

Solute injection into the natural sediments was carried out during the low ebb-water (soil was unsaturated) and monitored from 2 tidal cycles (Day-1) to Day-7. The positions of injection points (IPs) were marked using a 12-channel Garmin GPS76 marine navigator. At the expiration of each monitoring phase the respective locations of the IPs were identified and excavated carefully to penetrate the undisturbed plume domain. The design was such that each sampling point (SP) contains 3x5 IPs over 0.5mx0.5m square cells in 1.5mx2.5m rectangular arrays (see Fig. 2). Out of over 590x3 IPs initiated, a total of about 322x3 samples were successfully obtained, filmed/photographed (using Nikon Coolpix 8800 digital camera with 8.0 effective megapixels and 500MB storage capacity) and measured in the field.

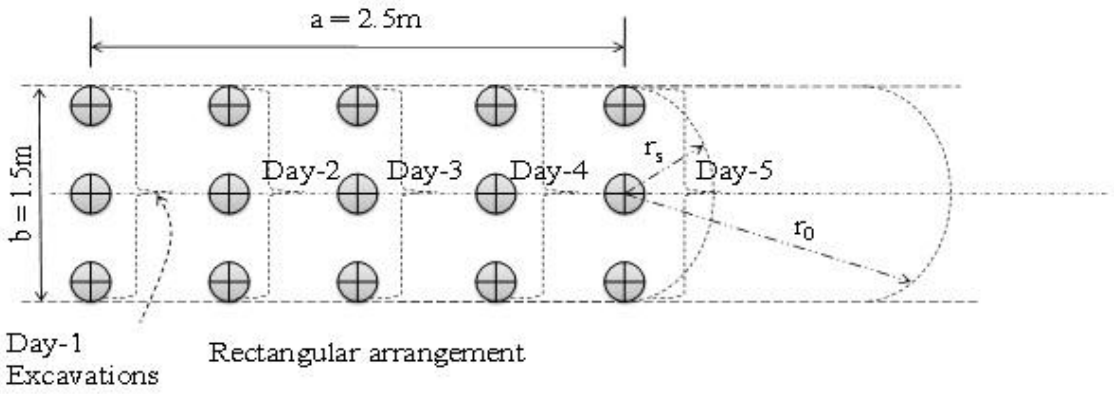

Figure 2: Arrangement of well points in a typical site in the field and daily excavation proceedure; r_s = distance at a point from the IP, r_0 = radius of influence, a function of the drawdown or drawup and permeability

The injectate is a Red Colour 810 permitted food solvent, colour (E124) with 4.3% pure dye content. A 5ml (0.215g) was injected using a 10ml syringe perpendicularly into the unsaturated natural beach-foreshore at the centre of 0.5m x 0.5m square cells (see Fig. 2), 0.05m below the surface. It was unable to measure the Day-7 plume-front widths as the spreading penetrated through the water table surface. The mean diameters, radius-ratios and areas of the plume were analyzed using the image processing tools, image-pro plus (IPP) and Matlab. The radius-ratio is a measure derived from taking the maximum radius of the plume divided by its minimum radius.

2.2.1 Digital-image processing

The spatial data were quantized by using the computer imaging techniques to convert the two-dimensional (2D) photo-images to digital formats with a $1/300^{th}$ pixels per inch resolution (Harrison, 1990; Russ, 1992). Concentration information was obtained from the tests conducted in the laboratory with dried samples of the beach-sand and related to the optical density intensity of the plume (Schincariol *et. al* 1993; McNeil *et. al* 2006). The concentration data were then obtained using the nonlinear indicial power relation $C = 0.3509 * \rho_{opt}{}^{5.3238}$ from the laboratory calibrations, where C is dye concentration; ρ_{opt} is the optical density intensity, $\left[\rho_{opt} = \log_{10}(m/I)\right]$, where *m* is a constant, and I (= (Red + Green + Blue)/3) is the light intensity (see Zhang *et. al* 2002 and Huang et. al 2002 for more details).

III. Mathematical Consideration

Following Tang and Babu (1979) and Chen *et al* (1999), the approximation to Bear (1972) equation for miscible displacement of conservative solute in porous medium can be described in cylindrical coordinates. The appropriate governing equation in cylindrical coordinates for radially convergent plume is:

$$\frac{\partial C}{\partial t} = \left(D_h \frac{r^2}{A^2} + \alpha \frac{r}{A} \right) \frac{\partial^2 C}{\partial t^2} - \frac{A}{r} \frac{\partial C}{\partial r} \qquad (1)$$

International Research Journal of Innovations in Engineering and Technology (IRJIET)

ISSN (online): 2581-3048

Volume 9, Issue 11, pp 99-116, November-2025

https://doi.org/10.47001/IRJIET/2025.911013

Where r is the radial coordinate, t is time, C is dye concentration, A is the area of plume, D_h is hydrodynamic dispersion coefficient, and α is the intrinsic dispersivity coefficient. D_h consists of the mechanical dispersion coefficient $D_{x'x'}$ and effective dispersion coefficient D_e, e.g. $D_h = D_{x'x'} + D_e$. The effective dispersion coefficient can be evaluated as $D_e = D_{em}/F\phi_e$, where D_{em} is effective molecular diffusion coefficient, ϕ_e is the effective porosity of soil (0.352±0.01) in the study site, and F is the resistivity formation factor and can be taken as 2.115±0.01 in the study area (Manheim *et al,* 2004).

Eq. (1) implies that the influence of dispersion and diffusion will decrease as distance-time ratios decreases in relation to the cumulative dispersive effect away from the injection source. The initial and boundary conditions of equation (1) can be specified from the field experiments as:

Initial condition: $C(r\neq 0, t=0) = 0$ (2)

Boundary conditions: $C(r=0, t) = C_0$, and $C(\infty, t) = 0$ (3a, 3b)

Where C_0 is the initial dye concentration at the origin of the cylindrical coordinate system.

With these initial and boundary conditions, the analytical solution of equation (1) is:

$$C(r,t) = \frac{M_0 / (\phi A_{plm})}{2} erfc\left(\frac{At/r^2 - 1/2}{f(r)} \right) \text{---------- (4)}$$

Where $M_0 = M_{000}$ = injected solute mass, A_{plm} = the cross-sectional area of the plume (the subscript plm refers to plume), ϕ is the porosity of the beach soil, *erfc* is error function and $f^2(r) = 1.33\frac{\alpha}{r} + \frac{D_h}{A}$. The zeroth moment ($M_{000}$) represents the spatial changes (migration and spread of a moisture plume) in moisture storage within the domain (Gee and Ward, 2001; Ye *et al.*, 2005).

The radial component of fluid in the porous medium is usually expressed as $Q/(2\pi\phi h_w r)$, where Q is volumetric rate of flow, and h_w is the depth from the water table to beach-sand surface.

The intrinsic dispersivity coefficient, α can be estimated by plotting $C(r,t)/C_0$ against $(1-\chi)$, where $\chi = 2A(t-t_{50})/r^2$, t_{50} relates to the time corresponding to $C(r,t)/C_0=0.5$. The hydrodynamic dispersion coefficient D_h has two main components, namely effective longitudinal coefficient D_L and transverse dispersion coefficient D_T. Individual calibration method for D_L and D_T was used to obtain D_L and D_T, thus D_h.

$X = (x - x_c)^2, Y = (y - y_c)^2$ assuming x and y are the visual sizes of the plume-pools x′ and y′ respectively. The effective dispersion coefficient however is evaluated using the radial distance, $r = (X^2 + Y^2)^{0.5}$. Where $r_c=(M_{100}/M_{000})$ mark the radial center of plume, $M_{100}=rC_r$, $M_{200}(r)=(r-r_c)^2C_r$ are the first and second order moments respectively, $\sigma_{rr}^2=(M_{200}(r)/M_{000})$ is the radiance and $C_r(r)$ refers to relative concentration as a function of the radius (Gee and Ward, 2001; Ye *et al.*, 2005).

Where the Gaussian Operator in Matlab $C(x) = ae^{\left[-((x-b)/\sigma_{x'x'})^2\right]}$ was applied, so that $D_{x'x'} = \sigma_{x'x'}{}^2/4t$, $\sigma_{x'x'}$= peak plume width, b = peak location of center of plume and $a = \left(\sqrt{4\pi D_{x'x'} t}\right)^{-1}$ = peak amplitude, and $D_{x'x'} = \frac{d}{dt}\left(\frac{M_{200}}{M_{000}} - \left(\frac{M_{100}}{M_{000}} \right)^2 \right)$ is proportional to the time rate of change of the spatial second moment of the concentration distribution with the first moment. Application of Eq. (2) will be made for comparisons with the results of calibrated concentration distribution models in a later paper.

IV. Results and Discussions

4.1 Solute plume transport

The morphology (tides) of the study area causes the water table to fluctuate hence the atmospheric pressure as the pore-water pressure rises and drops. The water table rises rapidly during floods but drains gradually even though the retreating flow tide may

International Research Journal of Innovations in Engineering and Technology (IRJIET)
ISSN (online): 2581-3048
Volume 9, Issue 11, pp 99-116, November-2025
https://doi.org/10.47001/IRJIET/2025.911013

be faster than the flow inland (Masselink and Hughes 1998). The varying patterns of elongation of the dye plume are described by analyzing the field observations which show the movement and transport with successive changes of tidal cycles.

4.1.1 Plume pattern observed at OEIS-IZ (A) and OEIS-IZ (B) during tidal cycles

All plumes at OEIS-IZ (A) and OEIS-IZ (B) were found to move downward vertically. Figure 3 represents a digital plume image showing the effect of beach morphology on the shape and distribution of the dye at OEIS-IZ (A). The interaction of groundwater table (GWT) and surface water table (SWT) due to pore-water pressure fluctuations generated by flood and ebb tides is thought to be major influence on the plumes. The flow of seawater into the unsaturated beach-sand can cause the beach water table to rise (Turner *et al* 1996). The conical shape plume is formed by the interactions of the plume and the infiltrated water, causing spreading and movement.

Figure 3: Sample of Day-1 (two-tidal cycles) plume image

The infiltration of water impacts the plumes in the beach subsurface causing attenuation which Philip (1973) described as a quasi-steady state condition. With infiltration, the pressure in the pore medium decreases as zones of low pressure is created at the impacted areas. The movement of the chemical pool was observed to be accompanied by pounding down effect where the bulk plume descends. The narrowing of the plume front with depth during the subsidence and elongation process indicates that the plume transits from the high conductivity to the low conductivity regions. However, during the ebb phase, there is a detachment at the interfacial layers of the beach groundwater table and the mean surface water. The tidal wave in the ground becomes distorted as a result of this behaviour due to the positive pore water pressure in the saturated sediments. Though the plumes continue to spread and subsidize in space and time, maintaining relatively upright position, their growth rather becomes stunted with increasing time-distance ratios towards the vicinity of the water table. Atypical example of hydraulic conductivity influence is shown in Fig 3, where the plumes generally widen at the top and the increasing tortuousity make the plume-fronts to narrow with the depth. This is clearly a physical demonstration of interstitial movement and transport of the dye plume.

4.1.2 Analysis of the observed plume development records

Fig. 4 shows a schematic illustration of the plumes at OEIZ-IZ (A) under the tidal forcing. A Cartesian coordinate system is established in Fig. 4 with x-axis along the beach surface and z-axis being in vertical direction. In Fig. 4, h_w is the depth of the ground water table, A_1 and A_2 are respectively the initial and final areas of the plumes after injection and excavation, Z_0 is the depth from the surface to the top of the plume; Y_0 is the depth from the surface to the centre of the plume; Y is the plume vertical size, W_1 is the plume horizontal size (top), and W_2 is the plume horizontal size (bottom). The measured data were analysed to

International Research Journal of Innovations in Engineering and Technology (IRJIET)
ISSN (online): 2581-3048
Volume 9, Issue 11, pp 99-116, November-2025
https://doi.org/10.47001/IRJIET/2025.911013

obtain the mean and standard deviation for each region using linear regression model in the window based statistical environment, statistical package for the social sciences (SPSS) version 17.

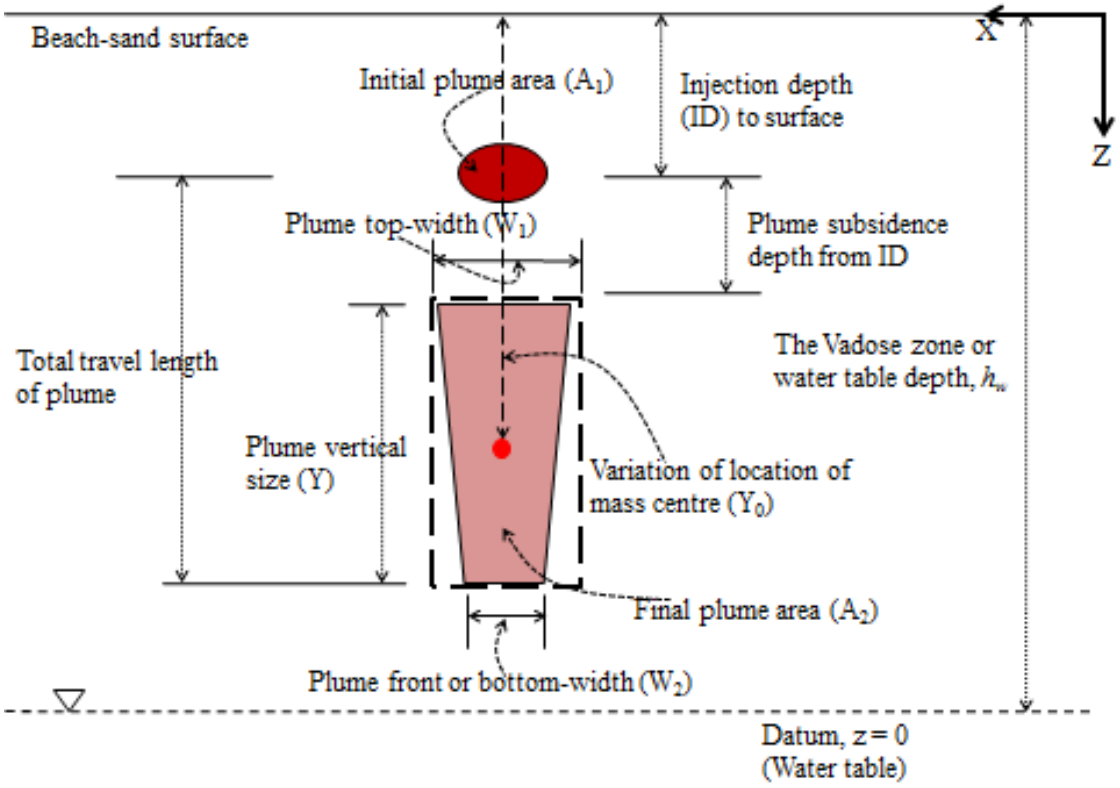

Figure 4: Illustration of plume and drawdown parameter development after tidal cycles

The vertical cross-sections of the conical plume-pools at both the OEIS-IZ (A) and the OEIS-IZ (B) terrains in the summer were found larger. This implies that the vertical cross-section of the dye plumes is the main direction of the groundwater flow (longitudinal transport) in this study. The vertical length of the cross section compared with its width varies according to the relationships $L_i \approx m_i W_{1i}$ and $W_{2i} \approx n_i W_{1i}$, where i = day-1, day-2, … and m, n are constants related to time. The vertical heights (Day-1, 2, …, 5) exceed W_1 by about m = 1.33, 1.76, 2.62, 2.02, and 2.16 times, while the $W_2$are$n$ = 0.398, 0.375, 0.431, 0.279, and 0.394 times the W_1 respectively. The radius-ratios obtained using the ratio between the maximum and the minimum radiuses accounted for the effective growth in the spreading of the plumes. The mean radius-ratio intervals and plume-pool areas for OEIS-IZ (A) (Sites-1, A) are listed in Table 1. Sharp contrasts of increasing radius-ratio intervals were observed when plotted against the center of the plumes (location of mass) for each zone (plot not shown). The trends of the radius-ratios demonstrate that the spreading rates relatively dampen at earlier times in OES-IZ (A), which could be partly attributed to the factor of subsidence. Furthermore, the hydraulic conductivity influence as the solute moves from the higher to the lower conductivity zones due to varying levels of moisture concentration and increasing constrictivity with depth could be another factor.

Though the differences of the plume widths and heights vary at each site, the general trend is found relatively identical from the analytical results shown in Figures 5-10. This suggests similarity of the characteristic properties of the sediments in the three regions (or sites), giving good indication of spatial variability. The mean data points in Figure 5 describe the variation of W_2 for sites-1, A and B. TheW_2observed in site -1 sharply decreases with depth up to day-3 and then significantly widens with time/depth. In site-A and site-B, slight delay before the upward concave variation curve is observed. This trend in the steady state transformation affecting the plumes indicates that the non-linear transitional movement exists. Similar behavior of the plumes in site-A and site-1 is observed and shown in Figure 6 which plots the variations of W_1 with time. In site-1, the plume top width W_1 has an initially slight decrease and then increases significantly from day-3 with an upward concave. The variation of W_1 in sites-A and B is somewhat complex. The plume top widths at both sites increase with time until Day 4. The plume top width at site-B then decreases sharply with time, while W_1 at site-A decreases slightly until Day 5 and then increases with time.

International Research Journal of Innovations in Engineering and Technology (IRJIET)
ISSN (online): 2581-3048
Volume 9, Issue 11, pp 99-116, November-2025
https://doi.org/10.47001/IRJIET/2025.911013

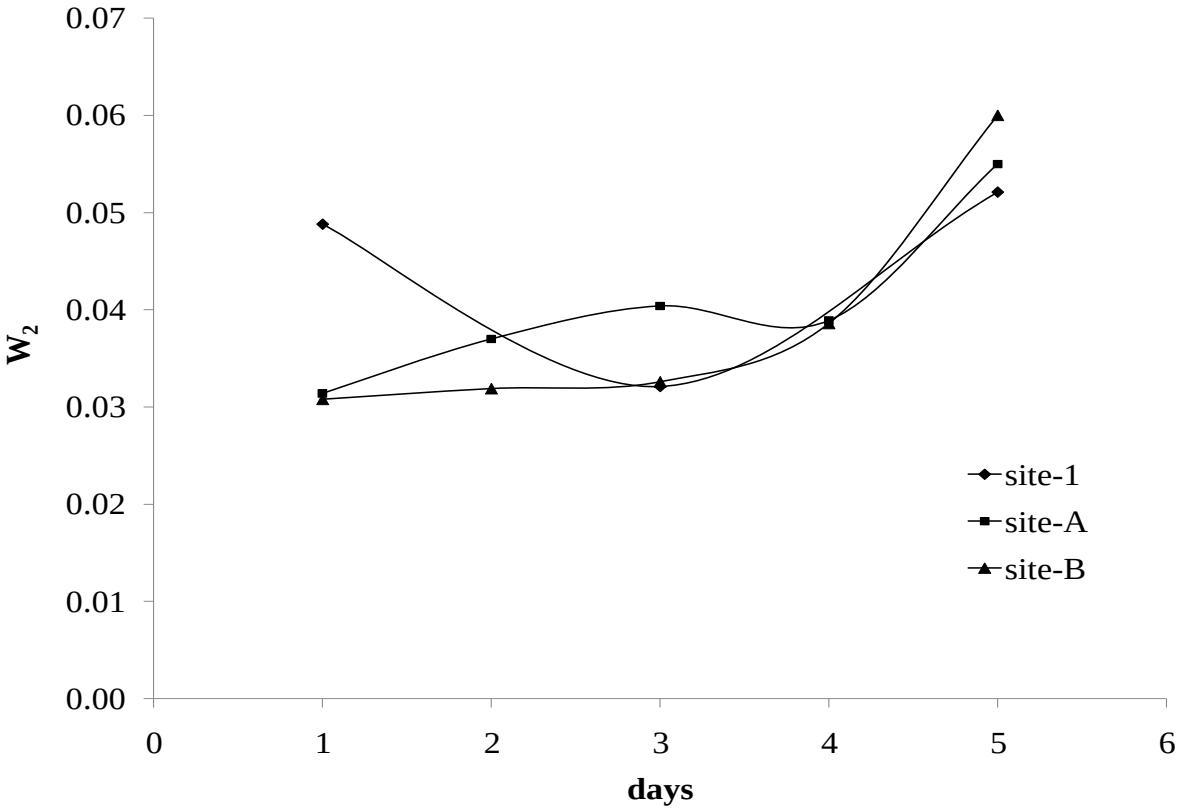

Figure 5: Comparisons of the variations of mean bottom widths of plumes in the three Sites (1, A & B)

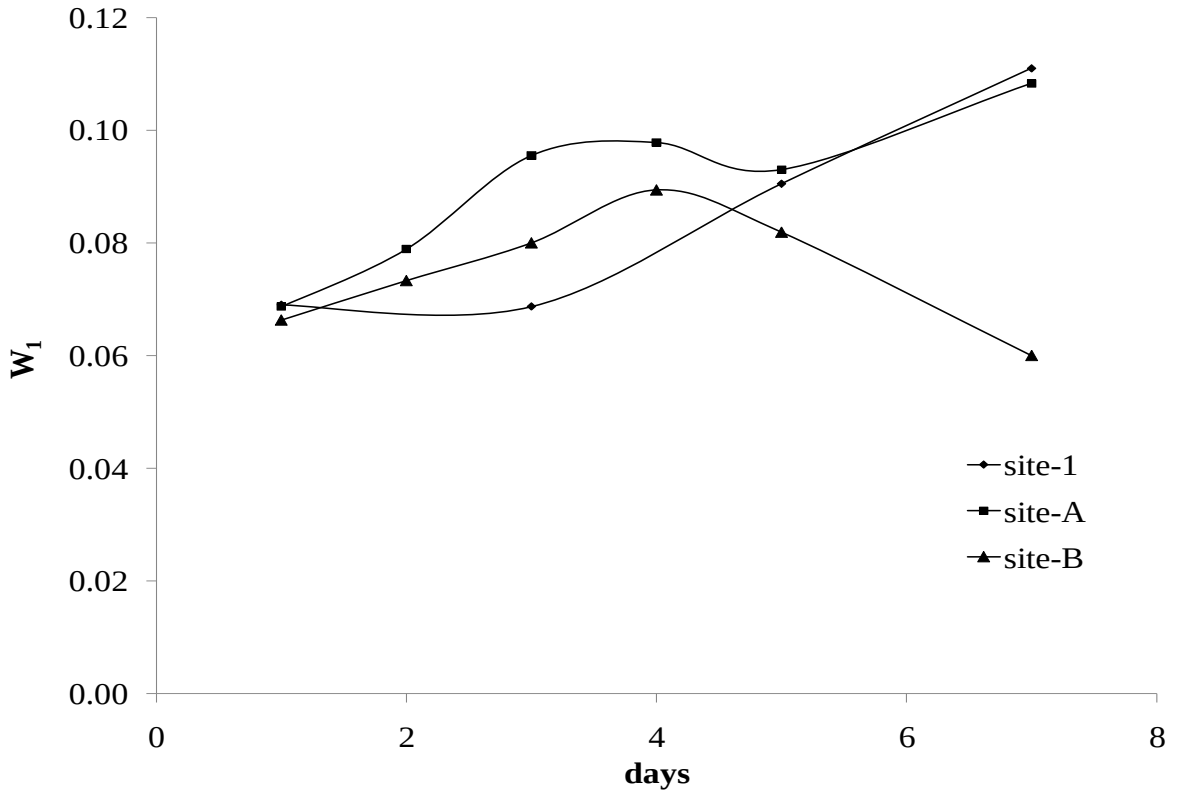

Figure 6: Comparisons of the variations of mean top widths of plumes in the three Sites (1, A & B)

International Research Journal of Innovations in Engineering and Technology (IRJIET)
ISSN (online): 2581-3048
Volume 9, Issue 11, pp 99-116, November-2025
https://doi.org/10.47001/IRJIET/2025.911013

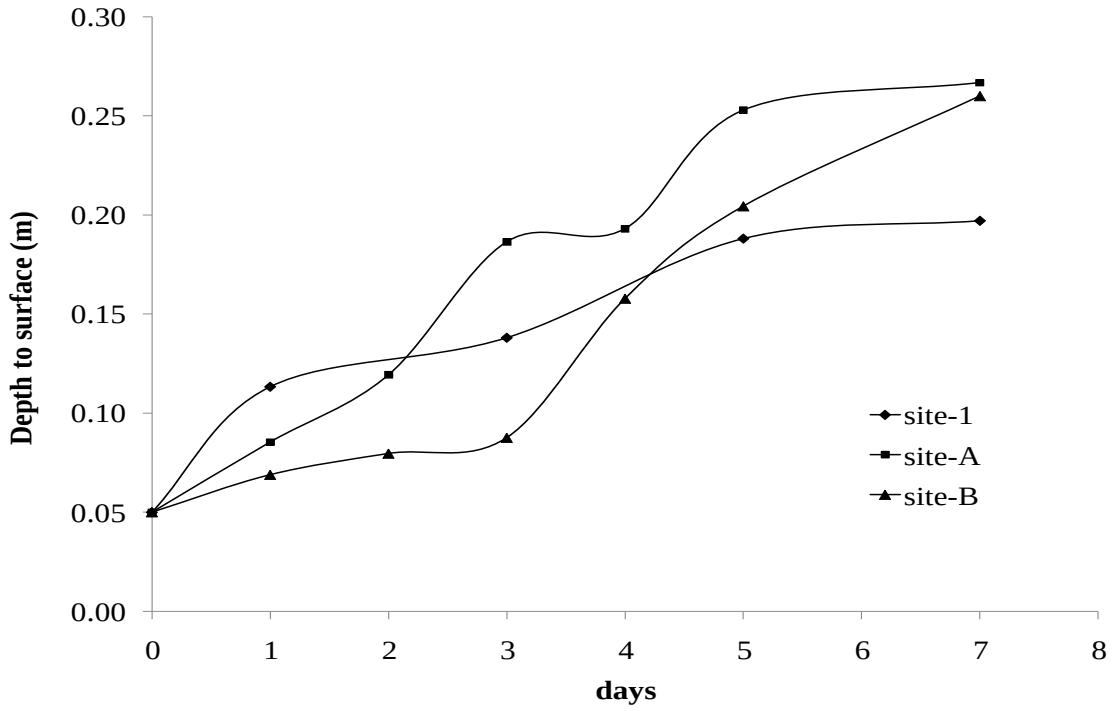

Figure 7: Observed mean variation of plumes in space away from the beach-sand surface with time (subsidence) compared in Sites 1, A & B

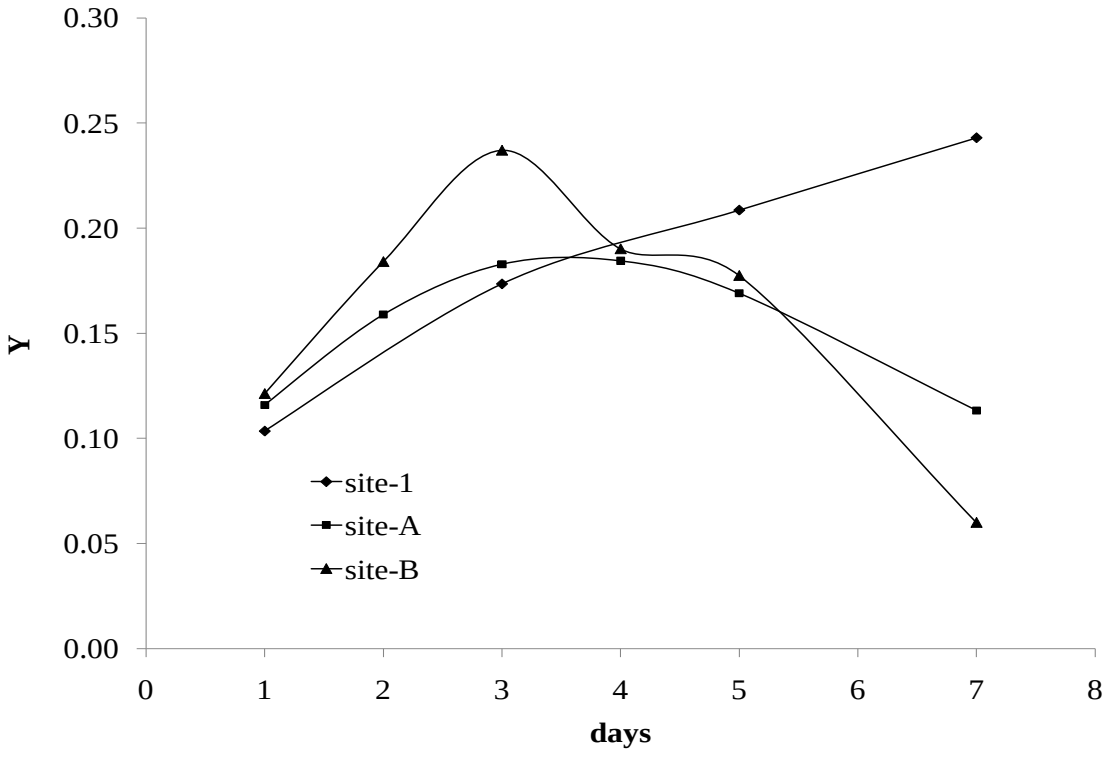

Figure 8: Comparisons of variations of mean vertical length of plumes in Sites 1, A & B

Figure 7 is the plot of the subsidence behavior of the plumes away from the sand surface for sites 1, A and B. In general, the depth to the sand surface in three sites increases with time though the movement of the plumes in three sites differs from each other. In site 1, the plume has a sharp downward movement in day 1 and then gradually mitigates downwards. An initial relatively sharp movement of the plume in site A takes place until day 3, followed by a gradual movement in day 4 and then sharp movement again. While in site B, the initial downward movement is gradual until day 3 followed by fast movement. The different movement characteristics of the plumes at three sites may reflect the differences of the groundwater table and sediment properties

International Research Journal of Innovations in Engineering and Technology (IRJIET)

ISSN (online): 2581-3048

Volume 9, Issue 11, pp 99-116, November-2025

https://doi.org/10.47001/IRJIET/2025.911013

at these sites. In Figure (8) we show the initial growth and subsequent decrease in the transport and elongation of the plumes. Physical and transport properties such as size distribution, density, tortuosity and porosity of the sediment can affect the spreading of the plumes induced by tidal load which could be associated to the downward concaves. The longitudinal growth of the contaminant is affected prominently from day 3 with decreasing trends. It is believed that in addition to the role of sediment properties in the field, the water table is also a factor of influence on the contaminants potential to spread as related earlier in previous sections. Figure 9 shows the variation of the distance from the plume center to the sand surface in sites 1, A & B with time. The plot shows that the longitudinal spread increases with the increase of time for all the sites. Figure 9 shows that a line well fits all data and represents the relative trend of all data points in three sites investigated. The trend shows that the data points are relatively associated to the dependent variable and that tidal variations (coastal dynamics) with time significantly influence the distribution. The center-line (linear model) is therefore a good statistical predictor of the outcome in this case.

Observations demonstrate the variation of the downward spreading of the plume center with time. The slope of the fitting line depends on the morphology of the terrain and sediment property and may relate to the transitional behavior of the tracer movement in the porous medium. The fast spreading of the plume center may be associated with the trap and release region where the tracer undergoes transition for further distribution along the mean flow. This region in the subsurface tends to weaken the course of spread relative to the water table depth and may need further study.

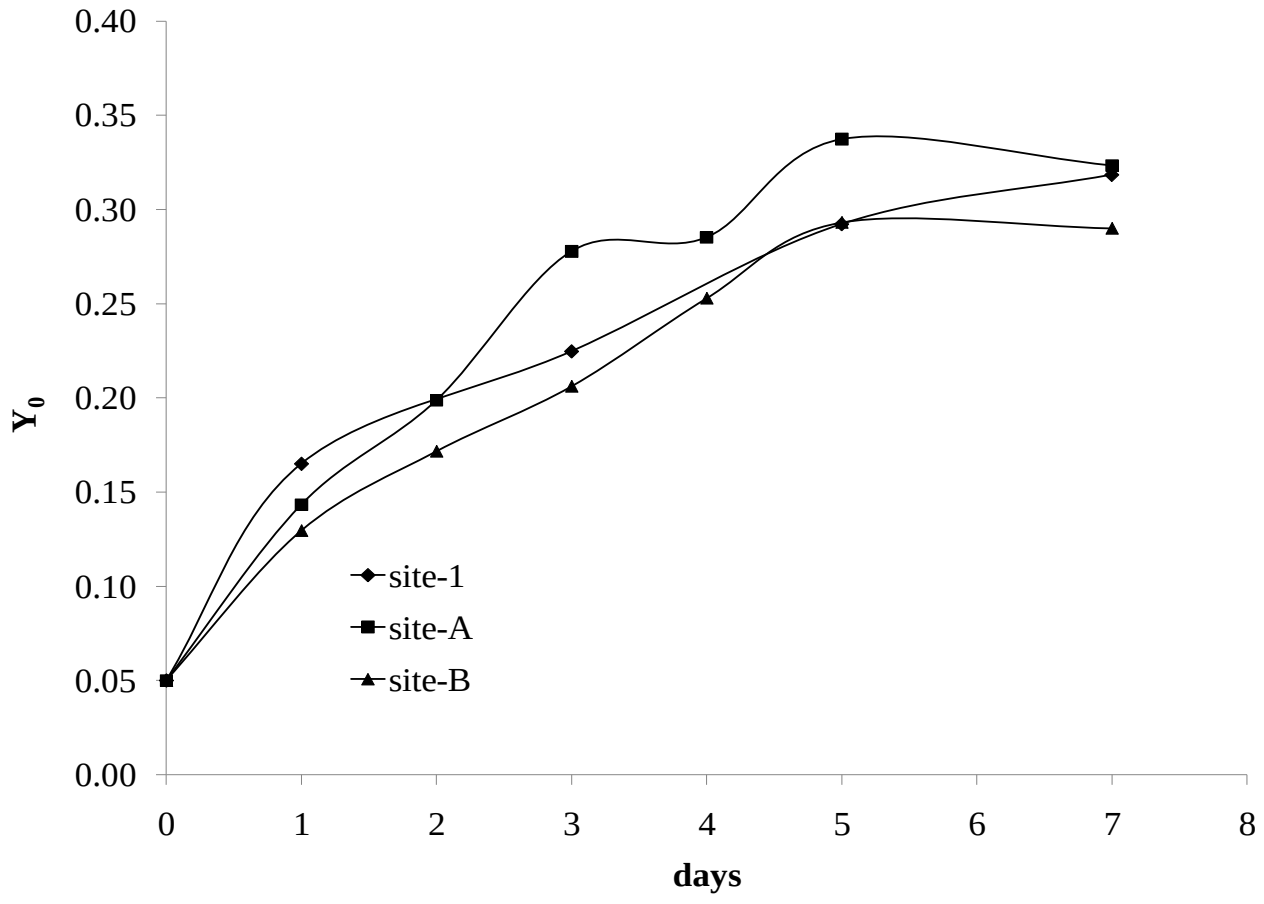

Figure 9: Variations of mean depth of plume centre of mass to surface compared in Sites 1, A & B

International Research Journal of Innovations in Engineering and Technology (IRJIET)
ISSN (online): 2581-3048
Volume 9, Issue 11, pp 99-116, November-2025
https://doi.org/10.47001/IRJIET/2025.911013

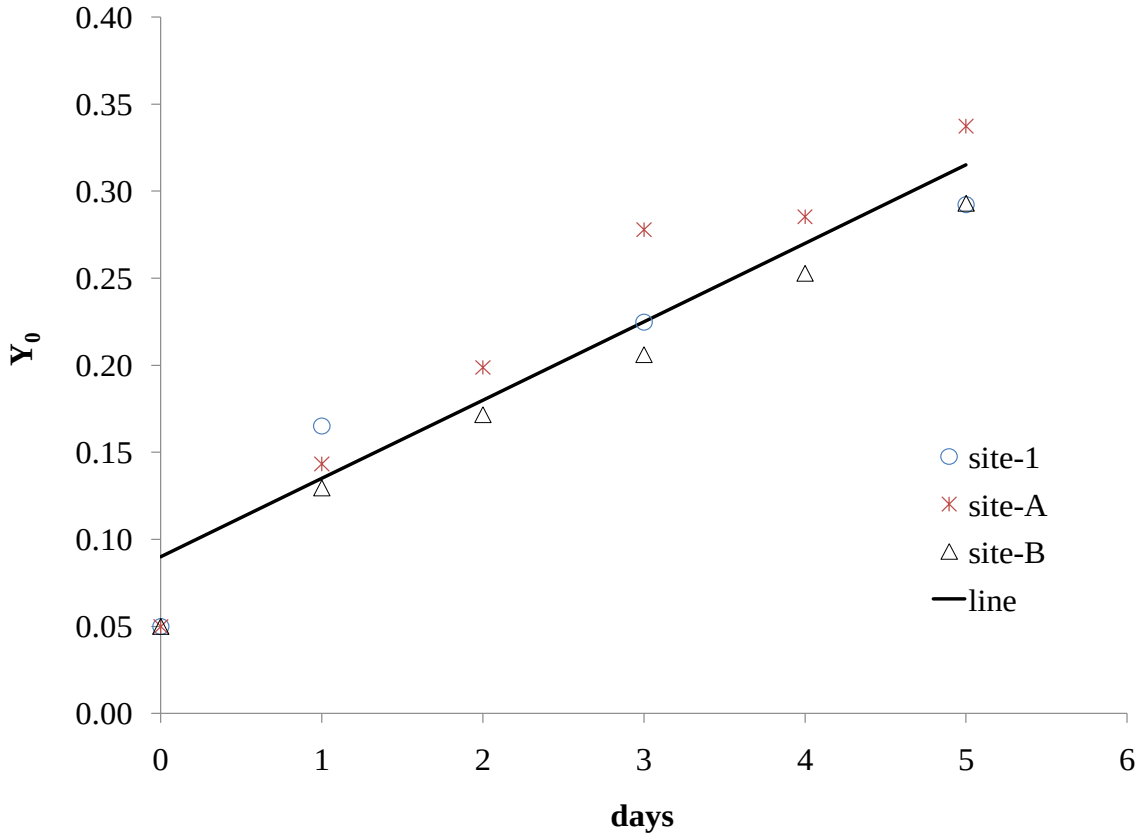

Figure 10: Linear model with line introducing rate coefficient affecting the centre of mass variation for the region (Sites 1, A & B)

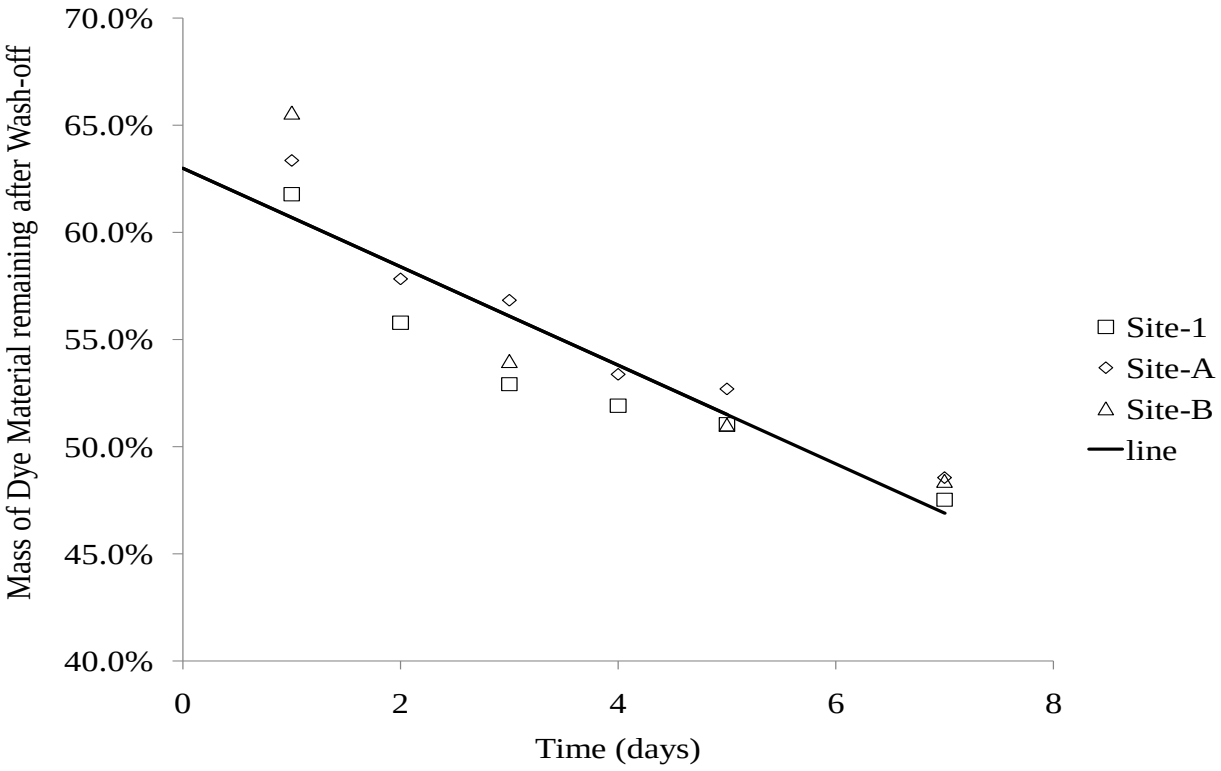

Figure 11: Linear model with line representing rate coefficient account for the effect of dye loss in the region (Sites 1, A & B)

Data points show estimated percentage of dye mass remaining with time after tidal surges.

International Research Journal of Innovations in Engineering and Technology (IRJIET)

ISSN (online): 2581-3048

Volume 9, Issue 11, pp 99-116, November-2025

https://doi.org/10.47001/IRJIET/2025.911013

4.2 Dye loss and rate coefficient effect

It is reasonable to assume that some percentage of the tracer dye will be lost to either the tide induced infiltrating surface water (during the flood phase) or groundwater as a result of the tidally induced interaction between the interfaces of the sediment/sand. This can be true since the dye concentration at the original point of the injection decreases during the tidally generated flux through the sediment. It is important to investigate the pertaining loading and attenuation (mass loss) in order to assess the stability of the induced contaminant plume for reliable environmental risk report. Fig 10 shows the results from integrating the non-equilibrium mass migration equation in the vertical space $\frac{dC_{solute}}{dt} = \gamma\phi_e / \rho_b$, where γ is the depth-dependent mass transfer coefficient and ρ_b is the bulk density of the sand. The spreading rate of the dye tracer can be estimated as 0.0834 m/day from the first-order moments estimate. It is seen from Fig. 10 that a significant loss (from about 35% in site B to 38% in site 1) of the dye mass takes place in the first day in all sites due to the action of the surface water and groundwater. The loss of dye mass then becomes gradual after day 2. The analysis of the data shows that the averaged value of γ differs in three sites, having a relatively lower value at Site-1 (0.0211) and Site-B (0.0229) and relatively higher value of 0.0273 at Site-A. Spatial and Dye Concentration Distributions of Plume-Pools

4.2.1 Solute advective velocity

The effective mean velocity in experimental sites was derived from plots using linear fits of first-order spatial moments versus elapsed time for the longitudinal cross-sections of the plumes (Itugha, 2008). The results show that the estimated velocity for the OES-IZ (A) zones being $3.475x10^{-3}$m/hr within 95% confidence bounds ($3.113x10^{-3}$, $3.838x10^{-3}$) while this velocity insite OES-IZ (B) is $1.512x10^{-3}$ m/hr. These values belong to the slow range (~$2.958x10^{-3}$m/hr) as suggested by Sudicky *et al's* (1983) in their groundwater aquifer based experiments. The import from the data in general reflects that higher conductivity sediments may likely enhance solute velocity than probable in borehole aquifer tests (Sudicky *et al*, 1983; Precht and Huettel, 2004; Ehrenhauss and Huettel, 2004). The velocities show that the surficial plane of the sand is likely the most affected by hydrodynamic events. This implies that pressure penetration into deeper horizons in the vadose zone may weaken with increasing depth as observed in 4.1.2.

4.2.2 Determination of dispersion coefficient and its relation with velocity

The hydrodynamic dispersion coefficient in the field sites, $D_h = D_{x'x'} + D_e$ can be evaluated using the field observations. The Gaussian model is applied to fit individual plume to determine D_h. Figure 11 shows the variation of the hydrodynamic dispersion coefficient with the location of the plume center at sites A and B. It is seen that the hydrodynamic dispersion coefficients at both sites increase linearly with the increase of the depth of the plume center away from the surface. The data shows that the gradients correspond to the mixing rates of the dye solution within the subsurface beach-sand. Fig. 11 shows the dependence of D_h on displacement influenced by local characteristic material and dispersity properties. Dispersity acts as an alternative mixing parameter related to the characteristic properties of the local beach-foreshore (Fried and Combarnous, 1971). It is also seen from Table 1 that the value of D_{er} is just about an order of magnitude less compared to D_h, implying that molecular diffusion cannot be ignored. This implies that the pore-scale mechanical dispersion and molecular diffusion have the potential to increase the diffusive transport at the RME with time.

As stated in section 3, the hydrodynamic dispersion coefficient D_h consists of the longitudinal (D_L) and transverse (D_T) coefficients. These two hydrodynamic dispersion components can be obtained from the Gaussian concentration distribution curves. The results show that D_L increase from $5.155x10^{-05}m^2$/hr to $9.375x10^{-05}m^2$/hr during the 5-days, while the transverse dispersion coefficient D_T varies from $5.770x10^{-06}m^2$/hr to $3.555x10^{-05}m^2$/hr. This shows that though the initial longitudinal dispersion coefficient is much larger than that in transverse direction, the two coefficients are in the same order after day 5. Given the relation between the flow velocity and dispersion coefficient, this implies that at the larger depth, the velocity in transverse direction is in the order of the longitudinal velocity. It is thought that the relative dominance of dispersion in the vertical plume cross-section is affected by low hydraulic conductivity zones encountered by the plumes during the subsequent variations of tidal head across the foreshore.

Comparing with the previous studies, the hydrodynamic dispersion coefficient found in this study favorably compares with those found by Pickens and Grisak (1981) and Dong and Selvadurai (2006, laboratory experiments) and is much smaller than

International Research Journal of Innovations in Engineering and Technology (IRJIET)

ISSN (online): 2581-3048

Volume 9, Issue 11, pp 99-116, November-2025

https://doi.org/10.47001/IRJIET/2025.911013

those obtained by Cho *et al* (2010), McNeil *et al.* (2006, laboratory experiments) and Garabedian *et al.* (1991) by two to three orders in magnitude. Another relevant study by Qian *et al.* (2009) has a broad range of dispersion coefficient whose lower value for small grain size is one order smaller than ours, while their high value for large grain size is five order larger than ours. These differences reflect the different experimental conditions (e.g. tidal induced forcing) and sediments.

During the few hours of active periods when the plume zones are stressed by tides, larger advection rates due to increase in dispersion will dominate mixing activity. This observation shows the marked increase in the dispersion coefficients with centre of mass location in each of the sampling locations (see Fig 11). It shows that the dispersion coefficient is dependent on the mixing rate induced spreading at any point and direction in the porous medium.

The asymmetry of the longitudinal cross-sections of the plumes implies the conditions supporting flow ponding. These processes can influence localized and dense accumulation stages in coastal beach sediments of the RME which promotes transport enhancement conditions such as large tidal amplitude, high sediment permeability, and shallow water depth. Relative anisotropic variations with depth can affect the distribution of concentration as dispersion is affected due to broader effects of velocity regimes opposed to constraints (Li and Ghodrati, 1995). The analysis shows that the dynamic exchange phenomenon between groundwater and surface water is restricted locally and is largely driven by semidiurnal tides synonymous with the study terrain, and this is responsible for significant flux activity at the outer RME beach. This is consistent with previous studies which found declining contaminants concentration in the sediments of the outer RME compared to the upper and inner estuaries. This can impact on traditional methods of releasing contaminants into coastal sediments and affect water quality management decisions, which may pose potential risks to catchment populations and ecosystems.

Furthermore, the variation of D_h with flow velocity is plotted in Fig. 12 (originally Fig. 13). It is seen that D_h in site B increases nearly linear with the increase of the velocity within the bounds of the vadose zone (i.e., between beach surface and water table), indicating that the mixing length (gradient) is almost stable as the plume-pool migrate in the beach-sand over the sampling period in site B. The relation between the hydrodynamic dispersion coefficient in site A and flow velocity is rather complicated. In general, the hydrodynamic dispersion coefficient in site A increases with the flow velocity though the data are rather scatter. The relation between the hydrodynamic dispersion coefficients and flow velocity is consistent with previous studies that shows that the dispersion coefficient is directly proportional to velocity (Perfect and Sukop, 2001; Perfect *et al*, 2002).

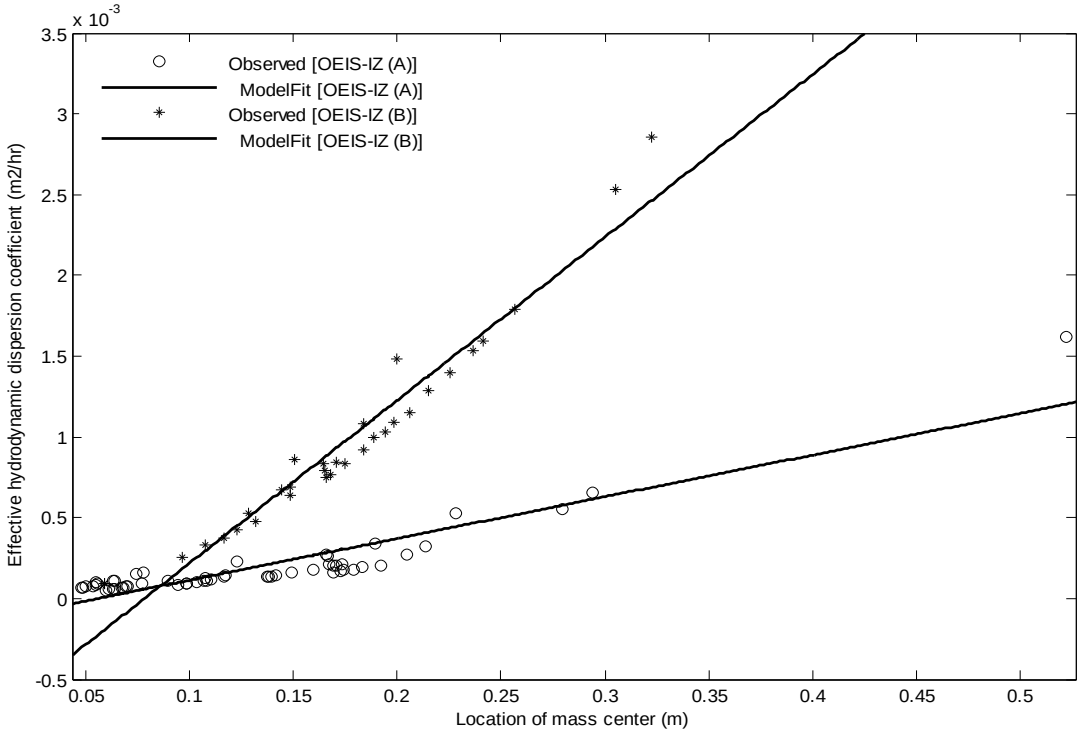

Figure 12: Least square fits for D_h dependence on the displacement plume center of mass in beach-sand

International Research Journal of Innovations in Engineering and Technology (IRJIET)

ISSN (online): 2581-3048

Volume 9, Issue 11, pp 99-116, November-2025

https://doi.org/10.47001/IRJIET/2025.911013

ModelFit [OES-IZ (A)] describes D_h varied by increasing linearly with distance [$D_h = 2.583x10^{-3}\,\bar{y}_c - 1.45x10^{-4}$; $R^2 = 0.8273$]; ModelFit [OES-IZ (B)] shows D_h increasingly varied linearly with distance by $D_h = 0.01009\,\bar{y}_c - 7.918x10^{-4}$; $R^2 = 0.9443$.

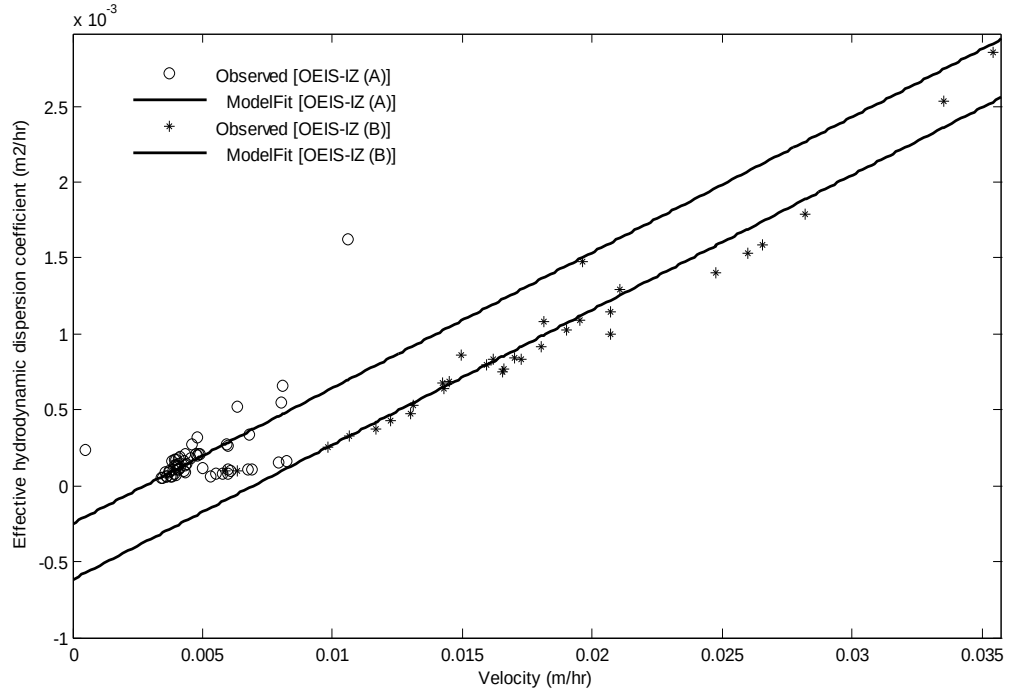

Figure 13: Linear dependence of D_h on velocity in relatively uniform undisturbed coastal beach-sand

ModelFit [OES-IZ (A)] describes D_h increasing linearly with velocity [$D_h = 0.08927v - 2.481x10^{-4}$; $R^2 = 0.3941$]; ModelFit [OES-IZ (B)] shows D_h linearly varied by increasing as velocity [$D_h = 0.08887v - 6.178x10^{-4}$; $R^2 = 0.$ 0.9544].

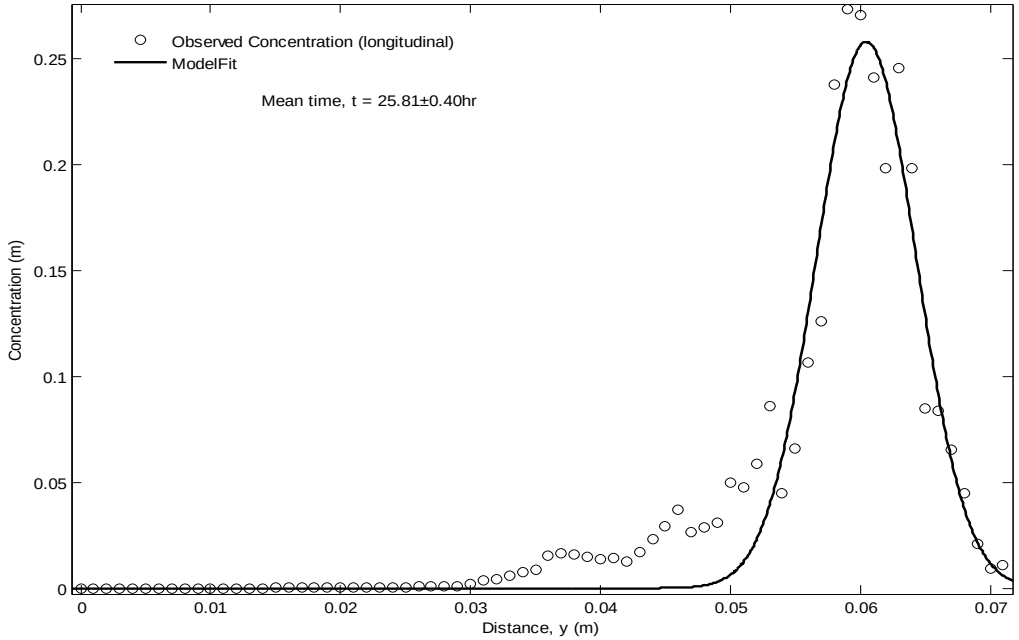

Figure 14: 1-D model showing asymmetry of transport (longitudinal) of observed concentration (circles) and fit (line) as a function of distance under natural oscillatory tides

International Research Journal of Innovations in Engineering and Technology (IRJIET)
ISSN (online): 2581-3048
Volume 9, Issue 11, pp 99-116, November-2025
https://doi.org/10.47001/IRJIET/2025.911013

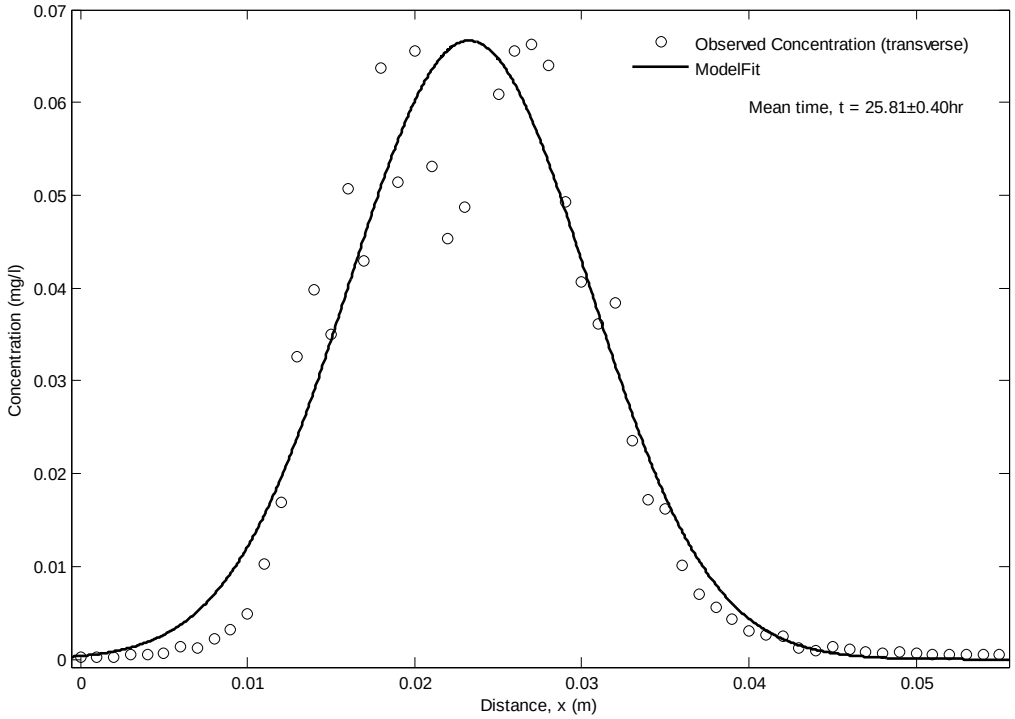

Figure 15: 1-D model symmetry showing the transport of contaminant concentration in the sediments as a function of distance under natural oscillatory tides, along flow the transverse to the vertical plane

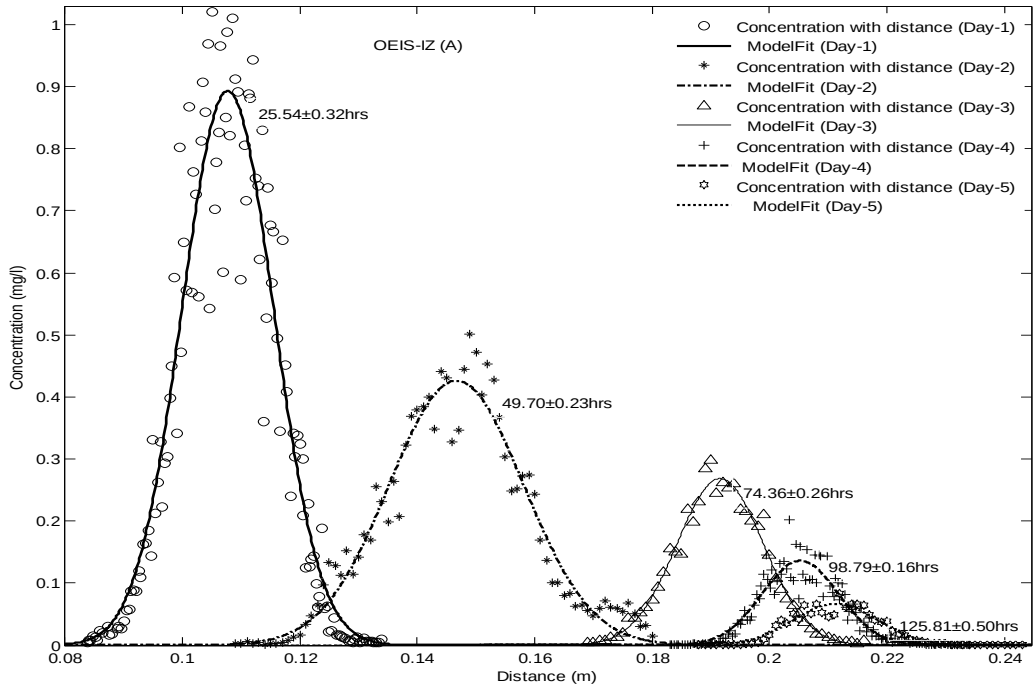

Figure 16: Comparison of observed and fitted concentrations with distance over time (transverse) for convergent tracer experiments in the summer for the durations of day 1, 2, 3, 4, 5at the OEIS-IZ (A) zone

International Research Journal of Innovations in Engineering and Technology (IRJIET)

ISSN (online): 2581-3048
Volume 9, Issue 11, pp 99-116, November-2025
https://doi.org/10.47001/IRJIET/2025.911013

4.2.3 Distributions of the plume concentration

The plume concentration is measured through the plume center in longitudinal cross section as well as in transverse cross section at different depths from the sand surface. Figure 13 (original figure 14) is the plot of the observed (open circles) vertical dye tracer concentration distribution in longitudinal cross section. The solid line in Figure 13 is the fitted line. It is seen from Figure 13 that the plume center (the maximum concentration) has travelled about 0.06 m away from the original inject position while the front of the dye plume has travelled to 0.07 m after day 1 (about 26 hours) of the injection. The measured result reveals that the spreading of the dye tracer concentration in longitudinal cross section is approximately a normal (the Gaussian profile) distribution. From the vertical concentration distribution the vertical spreading extent of the dye tracer can be estimated.

Figure 14 (original figure 16) shows the comparison of the observed dye concentration with the modeled dye concentration using equation (4) at various transport times indicated. The measured dye concentrations (symbols), which is measured through the plume center at various distances (times) from the sand surface, are normalized using the initial dye concentration. It is seen that the maximum dye concentration decreases as the plume disperses downwards into the deep sand while the dye concentration profile becomes flat with relatively wide peaks. This variation is associated with the increase of the transverse hydrodynamic dispersion coefficient with the depth from the sand surface. In general, the dye concentration distribution fits a Gaussian profile relative to the centroid of the plume in the transverse cross section at different depths away from the sand surface.

V. Summary and Conclusion

An image tool, the IPP and Matlab scripts have been successfully applied to process 2D color images of the chemical plumes monitored and observed in the RME subsurface foreshores. These analyzing techniques have enhanced the interpretation of the movement and transport of the plumes in the sediments. Over 300 groups of color maps were observed and analyzed to obtain to the concentration distribution profiles to characterize the dispersivity properties of the plume in sand beach subjected to the tidally induced forcing. From the observed movement of dye plume and analysis, the following conclusions can be drawn:

1) A procedure is developed for monitoring and observing the full field-scale plumes that maps GW flow paths under the influence of strong tides. The observed data are used to evaluate flow rates (pore velocity), dispersion, and concentration data with a view to determine GW flow direction and contaminants fate. The procedure unlike other field experiments (Precht and Huettel, 2004) is non-intrusive to obtain both the qualitative and quantitative data of the migration and transport process of the dye plume. The procedure uniquely centres on beach-sand vadose zone of the coastal foreshore in contrast to contaminant transport in groundwater aquifer studies. In addition, the method is uniquely different from previous studies where the injection position of the solute (source point) is different from the monitoring point.
2) The range of chemical plumes reported here, as due to strong hydrodynamic forces in sub-tidal beach-sand sediments, have not been seen in literature. The plumes show the persistent vertical conical gradients instead of the spherical/elliptical shapes widely reported in literature.
3) The variations in the high conductivity zone of the individual plumes (OEIS-IZ (A and B)) converge towards the water-table about the centerline, so that the concentration profiles expressed in the plumes pass through that zone showing sharp fringes with less spread. The visual account of the temporal and spatial variations between the top-widths and bottom-widths are presented with satisfactory evidence of plume response. The profiles of the vertical cross-sections of concentration distribution are related to local effect of the flow ponding and low hydraulic conductivity zones with localized and dense accumulation stages. The observed dye concentration distribution profiles in both the longitudinal and transverse cross section agree well with the Gaussian distribution.
4) The determined mixing rates and lengths with concentration distribution data are a source of water quality studies and represent the proof of greater dilution histories at the outer RME. The dynamic patterns of the plumes showed the vulnerability of not only the surface water and sediments but the groundwater, hence the food chain. This is important as it can improve the management decision on urban/industrial disposal mechanisms.
5) Further interpretation of the plume and terrain data can be made on industry standard ArcGIS which is useful in geoscience engineering studies.

A relatively large number of quantitative and qualitative datasets are obtained in this study using the developed method. These mined temporal and spatial plume data are difficult to achieve with invasive techniques in-situ (Precht and Huettel, 2004), and will be insightful and invaluable for validating the numerical models.

ISSN (online): 2581-3048
Volume 9, Issue 11, pp 99-116, November-2025
https://doi.org/10.47001/IRJIET/2025.911013

REFERENCES

[1] Baird, A. J., D. P. Horn (1996). Monitoring and modelling groundwater behaviour in sandy beaches. *Journal of Coastal Research*, 12(3): 630–640.

[2] Beinhorn, M., P. Dietrich, O.Kolditz (2005). 3-D numerical evaluation of density effects on tracer tests. *Journal of Contaminant Hydrology*, 81 (1-4): 89-105.

[3] Berkowitz, B., I. Dror, B.Yaron (2008). Contaminant Geochemistry: Interactions and Transport in the Subsurface Environment. *Springer-Verlag Berlin Heidelberg*.

[4] Boufadel, M. C., M. T. Suidan and A. D. Venosa (2006) Tracer Studies in Laboratory Beach Simulating Tidal Influences. *Journal of Environmental Engineering*, 132(6).

[5] Callaghan, P. T, S. L. Codd (1998). Generalised calculation of NMR imaging edge effects arising from restricted diffusion in porous media. *Magn. Reson. Imaging*, 16:471–8.

[6] Cartwright, N., L. Li, P. Nielsen (2004). Response of the salt–freshwater interface in a coastal aquifer to a wave-induced groundwater pulse: Field observations and modeling. *Advances in Water Resources* 27, 297–303.

[7] Chen, J. S., C. S. Chen, H. S. Gau, C. W. Liu (1999). A two-well method to evaluate transverse dispersivity for tracer tests in a radially convergent flow field. *Journal of Hydrology*; 223(3-4): 175-97.

[8] Cho, Yeo-M., D. Werner, K. B. Moffett and R. G. Luthy (2010). Assessment of Advective Porewater Movement Affecting Mass Transfer of Hydrophobic Organic Contaminants in Marine Intertidal Sediment. *Environ. Sci. Technol*., 2010, 44 (15): 5842–5848

[9] Diaw, E. B., F. Lehmann, Ph. Ackerer (2001) One-dimensional simulation of solute transfer in saturated–unsaturated porous media using the discontinuous finite elements method. *Journal of Contaminant Hydrology*, 51 (3-4): 197-213.

[10] Dong,W.andA. P. S. Selvadurai (2006). Image Processing Technique for Determining the Concentration of a Chemical in a Fluid-Saturated Porous Medium. *Geotechnical Testing Journal*, 29(5) 1-7.

[11] Ehrenhauss, S., M. Huettel (2004). Advective transport and decomposition of chain-forming plank tonic diatoms in permeable sediments. *Journal of Sea Research*, 52: 179–197.

[12] Fetter, C. W., (1999). Contaminant Hydrogeology. Second Edition, *Prentice Hall Upper Saddle River*, NJ 07458.

[13] Fischer, H. B., E. J. List, R. C. Y. Koh, J. Imberger, H. B. Norman (1979). Mixing in inland coastal waters. *Academic Press, London.*

[14] Fried, J.J., and M.A. Combarnous. (1971). Dispersion in porous media. *Soil Sci. Soc. Am. J.* 51:1434–1444.

[15] Garabedian, S. P., D. R. LeBlanc, L. W. Gelhar, and M. A. Celia, (1991). Large-scale natural gradient tracer test in sand and gravel, Cape Cod, Massachusetts, 2, Analysis of spatial moments for a nonreactive tracer, *Water Resources Research* 27(5): 911–924.

[16] Harrison, B.A., (1990). Introduction to Image Processing. *CSIRO Australia*, 256p.

[17] Huang, W.E., C.C. Smith, D.N. Lerner, S.F. Thornton, A. Oram (2002). Physical modelling of solute transport in porous media: evaluation of an imaging technique using UV excited fluorescent dye. *Water Research* 36: 1843–1853.

[18] Itugha, O.D. (2008). 'Solute and Particulate Transport at the Interface of Near-Shore Permeable Estuarine Beach-Sand: An Experimental Study of the Outer Reaches of River Mersey Estuary, NW England.' *PhD Thesis, The University of Liverpool, United Kingdom.*

[19] Itugha, O. D., D. Chen and A.A. Ahmed (2010).Solute migration and transport in coastal sand-beach sediments under strong tides. Vol. 2, 935-940. *In Environmental Hydraulics*.

[20] G. C. Christodoulou & A. I. Stamou (eds). *CRC Press, Taylor & Francis Group*, London, ISBN 978-0-415-58475-3.

[21] Jones, P. D., (2006). Water quality and fisheries in the Mersey estuary, England: A historical perspective. *Marine Pollution Bulletin* 53: 144–154.

[22] Khalili, A., A. J. Basu, U.Pietrzyk (1998). Flow visualization in porous media via Positron Emission Tomography. *Phys. Fluid* 10:1031–3.

[23] King, A.J., J.W. Readman and J.L. Zhou (2004). Determination of polycyclic aromatic hydrocarbons in water by solid-phase micro extraction - gas chromatography - mass spectrometry. *Analytica Chimica Acta* B, 523(2): 259-267.

[24] Lanyon, J. A., I. G. Eliot, D. J. Clarke (1982). Groundwater–level variation during semidiurnal spring tidal cycles on a sandy beach. *Aust. J. Mar. Freshwater Res.*, 33: 377-400.

[25] Li, H and J. J. Jiao (2005).One-dimensional airflow in unsaturated zone induced by periodic water table fluctuation. *Water Resources Research*, 41:W04007, doi:10.1029/2004WR003916.

[26] Li, L., D. A. Barry, F.Stagnitti, J.-Y.Parlange, D.-S. Jeng, (2000). Beach water table fluctuations due to spring-neap tides: moving boundary effects. *Advances in Water Resources*, 23: 817-824.

ISSN (online): 2581-3048
Volume 9, Issue 11, pp 99-116, November-2025
https://doi.org/10.47001/IRJIET/2025.911013

[27] Li, Y., M.Ghodrati (1995). Transport of nitrates in soils as affected by earthworm activities. *J. Environ. Qual.* 24: 432-438.

[28] Manheim, Frank T., David E. Krantz, and John F. Bratton (2004). Studying Ground Water under Delmarva Coastal Bays using Electrical Resistivity. *GROUND WATER—Oceans Issue* 2004 Vol. 42 (7): 1052–1068.

[29] Masselink G. and M.Hughes (1998). Field investigation of sediment transport in the swash zone. *Continental Shelf Research*, 18: 1179–1199.

[30] McNeil, J. D., G. A.Oldenborger, and R. A. Schincariol (2006). Quantitative imaging of contaminant distributions in heterogeneous porous media laboratory experiments. *J. Contam. Hydrol.*, 84: 36–54.

[31] Montemagno, C. D, W. G.Gray (1995). Photo luminescent volumetric imaging: A technique for the exploration of multiphase flow and transport in porous-media. *Geophys. Res. Lett.* 22:425–8.

[32] Nielsen, P. 1990. Tidal dynamics of the water table in beaches. *Water Resources Research* 26: 2127-2134.

[33] Perfect, E. and M. C. Sukop (2001). Models relating solute dispersion to pore space geometry: a review. In Physical and Chemical Processes of Water and Solute Transport/Retention in Soils. D. Sparks and M. Selim. Eds. *Soil Science Society of America Journal*, 56: 77-146.

[34] Perfect, E., M. C. Sukop and G. R. Haszler (2002). Prediction of dispersivity for undisturbed soil columns from water retention parameters. *Soil Science Society of America Journal*, 66(3): 696-701.

[35] Philip, J. R. 1973. Periodic non-linear diffusion: an integral relation and its physical consequences. *Australian Journal of Physics* 26: 513–519.

[36] Pickens, J.F. and G.E. Grisak (1981). Scale-dependent dispersion in a stratified granularaquifer. *Water Resources Research*, 17 (7): 1191-1211.

[37] Precht, E., M.Huettel (2004). Rapid wave-driven advective pore water exchange in a permeable coastal sediment. *Journal of Sea Research* 51: 93–107.

[38] Qian, Q, J. J. Clark, V. R.Voller and H. G.Stefan (2009). Depth-Dependent Dispersion Coefficient for Modeling of Vertical Solute Exchange in a Lake Bed under Surface Waves. *Water Resources Research*, 45: 1-13.

[39] Rahman, A., S. Jose, W. Nowak, and O. Cirpka (2005): Experiments on vertical transverse mixing in a large-scale heterogeneous model aquifer. *J. Contam. Hydrol.* 80: 130–148.

[40] Robbins, G. A. (1989). Methods for determining transverse dispersion coefficients of porous-media in laboratory column experiments. *Water Resource Research*, 25:1249–58.

[41] Rogers, H. R. (2002). Assessment of PAH contamination in estuarine sediments using the equilibrium partitioning–toxic unit approach. *Sci. Total Environ*. 290:139–55.

[42] Russ, J.C., (1992). The image processing handbook. *CRC Press Inc*, 445 p.

[43] Sahimi, M., (1995).Flow and Transport in Porous Media and Fractured Rock: From Classical Methods to Modern Approaches, *VCH, Weinheim*.

[44] Schincariol, R.A., E.E. Herderick, F.W. Schwartz (1993). On the application of image analysis to determine concentration distributions in laboratory experiments. *J. Contam. Hydrol*. 12: 197-215.

[45] Sudicky, E. A., J. A. Cherry and E. O. Frind (1983). Migration of contaminants in groundwater at a landfill: A case study, 4, A natural gradient dispersion test. *J. Hydrology* 63: 81-108.

[46] Swartz, C. H. and F. W. Schwartz (1998): An experimental study of mixing and instability development in variable-density systems. *J. Contam. Hydrol*. 34: 169–189.

[47] Tang, D. H. and D. K.Babu (1979).Analytical solution of a velocity dependent dispersion problem. *Water Resources Research*,15: 1471-1478.

[48] Turner, I. L., B. P. Coates and R. I. Acworth (1996).The Effects of Tides and Waves on Water-Table Elevations in Coastal Zones. *Hydrogeology Journal* 4(2): 51-69.

[49] Zhang, Q., R. E. Volker, D.A. Lockington (2002). Experimental investigation of contaminant transport in coastal groundwater. *Advances in Environmental Research*, 6: 229-237.

International Research Journal of Innovations in Engineering and Technology (IRJIET)

ISSN (online): 2581-3048

Volume 9, Issue 11, pp 99-116, November-2025

https://doi.org/10.47001/IRJIET/2025.911013

Citation of this Article:

Okuroghoboye Diepreye Itugha. (2025). Effect of Coastal Dynamics on Interstitial Hydraulics in Beach Sediments. *International Research Journal of Innovations in Engineering and Technology - IRJIET*, 9(11), 99-116. Article DOI https://doi.org/10.47001/IRJIET/2025.911013

****

